ADVANCED OPTICAL MATERIALS

www.advopticalmat.de

Plasmonic Gold Nanocones in the Near-Infrared for Quantum Nano-Optics

Assegid Mengistu Flatae, Francesco Tantussi, Gabriele C. Messina, Ahmad Mohammadi, Francesco De Angelis, and Mario Agio*

Plasmonic gold nanocones offer outstanding possibilities to control light-matter interaction at the nanoscale. For instance, they can be exploited to modify the photonic environment around a single emitter for tuning its quantum efficiency and radiative decay rate, as well as the angular distribution and polarization of the emitted photons. However, fabricating high quality nanostructures with the desired aspect ratio and tip radius of curvature is still challenging. Here, this study reports on the fabrication of high-quality plasmonic gold nanocones based on electron beam-induced deposition of an organometallic precursor on a substrate to define the structures, followed by sputtering deposition of a gold layer. The technique is versatile and has a very good spatial resolution for the fabrication of nanocones with dimensions in the 100 nm range and a small aspect ratio, while exhibiting a very sharp tip radius of curvature down to 6 nm. The nanocones are engineered to have resonances in the near-infrared region, where absorption in gold is smaller. Using single-nanoparticle spectroscopic techniques, this study characterizes their optical properties and measures the plasmon resonances, finding linewidths down to 50 nm.

1. Introduction

The manipulation of strongly localized optical fields to control light-matter interaction finds a wide range of applications in information processing,[1] lithography,[2] sensing,[3,4] spectroscopy,[5] and microscopy.[6] On a more fundamental level, it has implications for instance in cavity quantum electrodynamics.[7,8] For these studies, researchers have made extensive use of dielectric micro- and nanostructures, such as micropillar resonators,[9] whispering-gallery-mode resonators,[10] and photonic-crystal cavities.[11] Recently, there has been a huge interest to engineer the photonic environment using plasmonic nanostructures,[12–22] because they exhibit localized surface plasmon resonances (LSPR) that lead to tiny mode volumes in the confined near field. Moreover, they can be easily tuned by changing the size and shape of the nanostructure or enhanced by introducing sharp features that produce even stronger localized electromagnetic fields (the so-called lightning rod effect). Finally, plasmonic nanostructures have relatively broad resonances, which can easily match the emission spectrum of emitters at room temperature, like quantum dots, color centers in diamond, and fluorescent molecules.[23–25]

Theoretical calculations have shown that plasmonic gold nanocones are particularly interesting for these purposes.[26] On the one hand, a single nanocone provides more than three orders of magnitude enhancement of the radiative decay rate, while keeping the antenna efficiency larger than 80% (for an electric dipole source, with unity quantum yield, oriented along the symmetry axis of the nanocone and placed at a distance of 10 nm from the tip with a radius of curvature of 10 nm).[26] On the other hand, sharpening the tip can further enhance the confined optical field (hotspot), while resonance wavelength and radiation efficiency can be tuned by adjusting base and height. However, these performances demand a high manufacturing precision (e.g., aspect ratio, sharp tip, right-circular conical shape, and inclined side wall), especially for studies on single emitters, which makes the fabrication process of these 3D structures very challenging.

Recently, researchers have shown different approaches to fabricate plasmonic gold nanocones. Fleischer et al. have developed a technique using thin-film deposition of gold, followed by an etch mask developed on the gold film using electron beam (e-beam) lithography, and subtractive ion milling.[27] The ion bombardment of gold leads to the formation of conical shapes with the cone axis pointing along the direction of ion incidence, while the nanocone side wall is determined by the etch mask erosion and the angle-dependent sputtering yield. The final cone angle is given by the sputtering process of the sidewalls (not the lateral erosion of the etch mask) and the cone base by the angle of maximum sputtering yield (not by the mask diameter). Hence, controlling the size (base and

Dr. A. M. Flatae, Dr. F. Tantussi, Dr. G. C. Messina, Dr. F. De Angelis
Plasmon Nanotechnologies
Istituto Italiano di Tecnologia
16163 Genova, Italy
E-mail: flatae@physik.uni-siegen.de
Dr. A. M. Flatae, Prof. M. Agio
Laboratory of Nano-Optics
University of Siegen
57072 Siegen, Germany
Dr. A. Mohammadi
Department of Physics
Persian Gulf University
75196 Bushehr, Iran
Prof. M. Agio
National Institute of Optics (INO)
National Research Council (CNR)
50125 Florence, Italy

DOI: 10.1002/adom.201700586

height) and the shape relies on a lot of parameters. Hsu et al. have fabricated conical nanostructures by self-assembly of nanoparticles and etching.[28] Silica (SiO_2) nanoparticles are deposited on silicon (Si) by Langmuir–Blodgett assembly (as a mask) and the mask is shrunk by isotropic reactive ion etching (RIE) of SiO_2. The anisotropic etching of Si into pillars by RIE followed by removal of the residual mask by hydrofluoric (HF) etching leads to conical shapes. Geometry and sharpness of the nanocone are controlled by the etching conditions. By this method selective fabrication of nanocones at a desired place is challenging. Hoffmann et al. have demonstrated the fabrication of nanocones using focused ion beam (FIB) milling of a sputtered nanocrystalline gold layer.[29] This is a multistep cumbersome FIB etching process that needs different ion beam properties for the removal speed of each processing stage and patterning resolution. This method is also not suitable for large scale fabrication. Wu et al. have obtained nanocones based on a nanoimprint lithography (NIL) (stamping technique).[30] First, silicon nanocones made by Bosch etching process (master mold) are pressed into a polymer layer to create negative cones (daughter mold). Then, other polymer cones are imprinted from the daughter mold and then coated with gold. Polymer nanocones and reversed polymer cone molds are fabricated using ultraviolet (UV) curable NIL and can be subjected to volume shrinkage during UV curing. Therefore, a proper NIL resist is the key for achieving a good structure. Nanocones fabricated with this approach require adequate mechanical stiffness of the polymer. In a 3D structure, the softer the mold, the more the pattern will tend to deform. Moreover, the fabricated nanocones do not present a defined circular shape and exhibit multiple tips, which make them not suitable for coupling single emitter as fabrication precision is mandatory to achieve the theoretically expected values. Kontio et al. have demonstrated the fabrication of nanocones based on a combination of UV-NIL and e-beam evaporation.[31] UV-NIL and RIE are used to replicate a pattern of high aspect ratio cylindrical holes. Then a gold layer is deposited by e-beam evaporation until the holes are filled. In most cases evaporation into the holes spontaneously form nanocones. It is reported that the conical shape is formed spontaneously when the cylindrical holes in the mask shrink during evaporation. A disadvantage of this method is that there is no easy way to control the radius of curvature of the nanocone and the deposited metal structures are grainy. The sharpness and the final height of the cone depend on the evaporated material. A material with good adhesion to the etched lift-off structure defines a shrinkage-rate of the hole in the mask. Kim et al. have fabricated nanocones using nanotransfer printing.[32] A master (template) cone is prepared by photolithography or e-beam lithography, from which a mold is replicated and then gold is deposited. The final structure is obtained by pressing and demolding on a substrate. This method is cheaper but do not produce sharp features as required.

In this paper, we show the fabrication and optical characterization of high-quality plasmonic nanocones that are suitable for the study of light-matter interaction in quantum nano-optics. The nanocones are fabricated using an electron beam-induced metal deposition (EBID) technique. The e-beam is favored to the FIB as it provides a smaller spot (achieving better focusing and resolution) and avoids FIB-induced reactions that lead to (gallium) contamination inside and nearby the deposited material. Similar approach using EBID and FIB milling for the fabrication of high aspect ratio gold pillars was reported by De Angelis et al.[33]

Unlike the previously discussed methods, our fabrication process offers a good control over the size, shape, and radius of curvature of the nanocones. It also provides individually tailored structures that can be fabricated on any substrate in a position-controlled manner without any masks. The technique is also versatile and has a very good spatial resolution for the fabrication of nanocones with small aspect ratio while maintaining a very sharp tip radius of curvature. This is particularly useful where precision in fabrication of single nanostructures is a fundamental issue. Moreover, thanks to the short exposure time (few seconds) required to fabricate a single structure, our technique provide an alternative method of fabrication for other applications that require multiple arrays of well-defined nanocones.

The nanocones are engineered to have resonances in the near-infrared region (NIR), where less investigations have been made so far. The NIR range is of our interest for several reasons. First, absorption in gold is smaller in the NIR (also resulting in a smaller relative intrinsic linewidth of the LSPR). Second, the emission of some of the best photostable quantum emitters (e.g., silicon, nickel, and chromium related color centers in diamond) are in the NIR region. In addition, this spectral region is also interesting for biomedical applications as tissue is more transparent in the NIR. Finally, nanocones with NIR resonances are attractive for exploring strong-field phenomena in nanosystem.

Using a homemade single-nanoparticle spectroscopy setup, we have optically characterized the nanocones and their resonances in the NIR. Further theoretical calculations focused on the fabricated geometries confirm that nanocones can indeed considerably enhance the emission rate of quantum emitters, while keeping a large quantum efficiency.

2. Results and Discussions

2.1. Dark-Field Imaging and Spatial Resolved Intensity Measurements

Figure 1a depicts an optical image of nanocones under dark-field illumination. Using the horizontal dimension of the charge-coupled device (CCD) pixel array of the camera, we have counted the number of scattered photons from a single nanocone and compared the scattered signal with the background (spatially resolved photon counting). Figure 1b (lower panel) shows the intensity of the scattered signal corresponding to a horizontal cut across two nanocones (upper panel). It compares the scattered light intensity of two nanocones with the background. It is found that in our excitation scheme the scattered signal is about 73 times stronger than the background and intense enough to be detected by the spectrograph.

A small defocusing of the optics (≈200 nm–1 μm) allows direct determination of the dipole emission pattern based on the intensity distribution of the defocused image.[34] By defocusing the objective, a doughnut shape of the scattered field is observed for nanocones excited by p-polarized light. This is

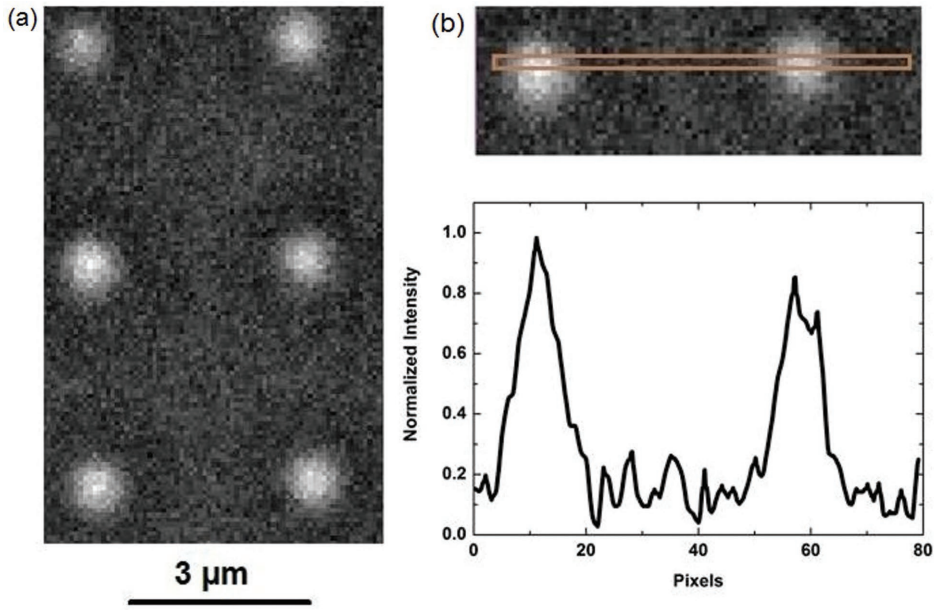

Figure 1. a) Dark-field scattering image of gold plasmonic nanocones. b) Scattering signal (lower panel) corresponding to a horizontal cut across two nanocones (upper panel).

characteristic of a dipole oriented along the longitudinal axis (height) of the nanocone and indicates that the longitudinal mode of the nanocone is excited. **Figure 2**a shows a defocused dark-field image of a nanocone under p-polarization. Using the vertical CCD pixel array of the electron multiplying CCD (EMCCD), we have determined the spatial intensity distribution of a cross-section along the vertical line through the center of the pattern. As depicted in Figure 2a, the doughnut shape of the scattered field is characterized by a bright ring with a dark center, corresponding to the excitation of the longitudinal plasmonic mode. When the nanocone is excited by s-polarized light instead of the doughnut shape the spatial intensity profile in Figure 2b shows a Gaussian-like intensity pattern. This is attributed to the excitation of transverse mode.

2.2. Resonance Spectra of Plasmonic Gold Nanocones

To obtain LSPRs in the NIR region, we have chosen gold nanocones of gold layer thickness 30 nm with base diameter in the range of 110–120 nm and aspect ratio (height to base) of 1–2. The LSPR peak redshifts with increasing nanocone height and blueshifts when increasing the base diameter. Therefore, by tuning the aspect ratio we find the LSPR at the desired spectral position. **Figure 3**a shows the LSPRs of individual nanocones for different aspect ratios.

The LSPR is a manifestation of a coherent oscillation of the conduction electrons of the nanoparticle. The linewidth Γ of the LSPR depends on the shape, size, surrounding environment, and type of substrate used. The main mechanisms that determine the linewidth at resonance are energy loss via coupling to the radiation field (radiation coupling), electron-surface scattering and the relative contribution from bulk dephasing. Formally, it is defined as $\Gamma = \Upsilon_b + (A v_f / l_{eff}) + 2\,\hbar\,\kappa\,V$ where, Υ_b is the bulk damping constant, A is a constant that depends on the detail of electron-surface interaction, v_f is the Fermi velocity of electrons, l_{eff} is the effective path length of the electrons, κ is a constant that characterizes the efficiency of radiation damping, and V is the volume of the nanostructure.[35,36] The first two terms corresponds to bulk damping and electron-surface

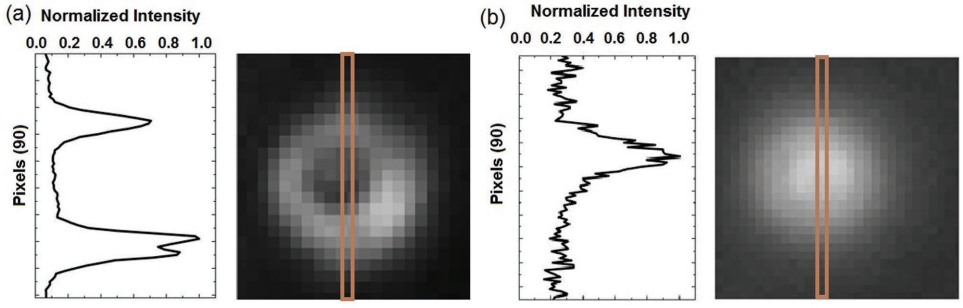

Figure 2. a) Dark-field image of a slightly defocused nanocone under p-polarized illumination shows doughnut (ring) shape intensity distribution. b) Dark-field image of a slightly defocused nanocone under s-polarized illumination shows a Gussian-like scattered field profile.

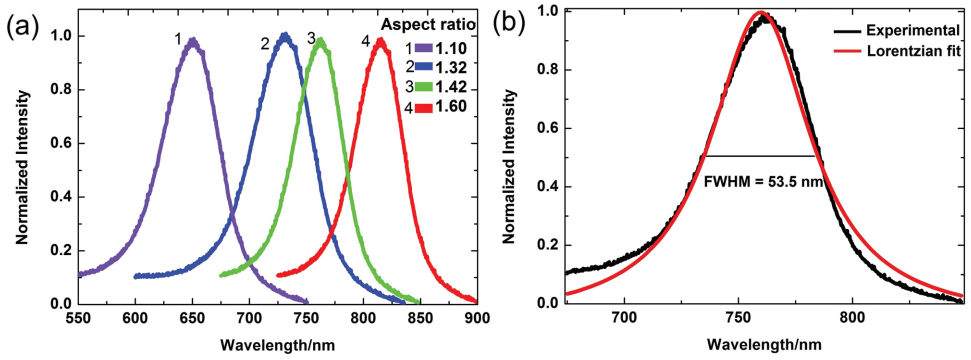

Figure 3. a) LSPR spectra of gold nanocones for various aspect ratios. b) The linewidth of the LSPR can be as small as 53.5 nm.

scattering respectively, and are a dominant process for nanostructures below 20 nm.[35,36] For larger sizes, for instance in our case, radiation damping is the most significant dephasing process that determines the linewidth. This is mainly because radiation damping is proportional to the volume of the nanostructure, whereas electron-surface scattering is inversely proportional to it.

In our gold plasmonic nanocones the LSPR linewidth is found between 50 and 70 nm (see Figure 3b), which is relatively narrow as compared to previous reports in the visible wavelength range.[6,29] This can be attributed to two basic phenomena: (i) although radiation damping is the main dephasing process, it scales with λ^{-3} and thus becomes smaller in the NIR;[36–38] (ii) the absorption losses of gold are smaller in the NIR region.[39–42]

Following the above discussion, a dephasing time T of about 7–10 fs can be roughly deduced from the linewidth Γ according to $T = 2\ \hbar/\Gamma$ and $1/T = \kappa\ V$, where Γ is defined in units of energy (eV). Analysis of the linewidth data shows the radiation damping parameter $\kappa = (3.2 \pm 0.6) \times 10^{-7}$ fs^{-1} nm^{-3} in agreement with previously reported values for gold nanostructures of similar size.[43] The quality factor Q (that is the measure of the number of oscillation a LSPR undergoes before its decay) is in the range of 10–15. It determines the resonant enhancement of the local optical field intensity ($\approx Q^2$), (i.e., 100–225 fold enhancement in our case). For a process like surface-enhanced Raman scattering, the enhancement scales as Q^4 (i.e., 10^4–5×10^4). Optimization of other geometrical parameters (e.g., a sharper tip) can further increase the field enhancement.

3. Conclusions

In summary, we have presented the fabrication and optical characterization of high-quality plasmonic nanocones obtained through focused electron beam-induced deposition technique followed by gold layer deposition. Our fabrication allows a precise control over the nanocone base, height, radius of curvature, and side wall. These results are quite promising for the fundamental study of light-matter interaction in quantum nano-optics, where a high fabrication precision is required. Moreover, we have been able to tune the LSPR in the near-infrared spectral region, which has been so far poorly explored for nanocones, despite the great interest in quantum nano-optics. We have in particular discussed that the structure can be suitable for enhancing the total (radiative) decay rate of a quantum emitter by more than two orders of magnitude, while keeping a large antenna efficiency. The antenna efficiency further increases with the thickness of the gold layer as the interaction between the platinum–carbon core and LSPR decreases. On the other hand, the radius of curvature tends to increase for large gold thicknesses. The sharpness of the nanocone tips could be improved by optimization of the gold evaporation and annealing process, especially for thicker gold coatings. Finally, the LSPRs exhibit a relatively narrow linewidth (about 50 nm) with a plasmon dephasing time of around 10 fs. These nanocones may also find applications in spectroscopy, field emission, and attosecond science.[44–48] In addition platinum nanocones may also be interesting for nanocatalysis, e.g. to improve electron-transfer reactions and determine the activation energy without being consumed in the process.[49]

4. Experimental Section

Fabrication: The substrate, a chemically and mechanically robust 100 nm thick silicon nitride (Si_3N_4) membrane (dimension 500 µm × 500 µm) suspended on a silicon frame, was washed in acetone, rinsed in isopropyl alcohol, and finally cleaned in oxygen plasma at a power of 100 W for 2 min. Then, 10 nm gold layer was deposited on the membrane in order to avoid charging effects during the exposition to the e-beam, which can lead to deflection, distortion, and defocusing of the incoming e-beam.

A FEI Helios Nanolab 600 DualBeam system (combining a scanning electron microscope and focused ion beam (SEM/FIB) in one instrument) is used for the EBID. The system is equipped with a gas injection system that enables focused beam-induced deposition. At first, an organometallic platinum (Pt) precursor, (trimethyl)methyl cyclopentadienyl-platinum (chemical formula $(CH_3)_3(CpCH_3)Pt$), is fluxed trough a fine capillary (needle) inside the vacuum chamber in close proximity to the surface of the substrate, where the gas is adsorbed on the sample surface. As a precursor, platinum-containing gas is preferred as it allows a high deposition rate and precision. Furthermore, it is chemically resistant, free of any cross contamination and the conducting metallic nature of the later deposited platinum allows live imaging of the fabricated nanostructure. The focused e-beam (working at an accelerating voltage of 10 kV and a dose current of 100 pA) scanning over the substrate defines the nanocones. The scanning process is computer controlled and the deposition rate depends on the processing parameters: the residual vacuum pressure (10^{-9} Torr), the pressure during deposition (the

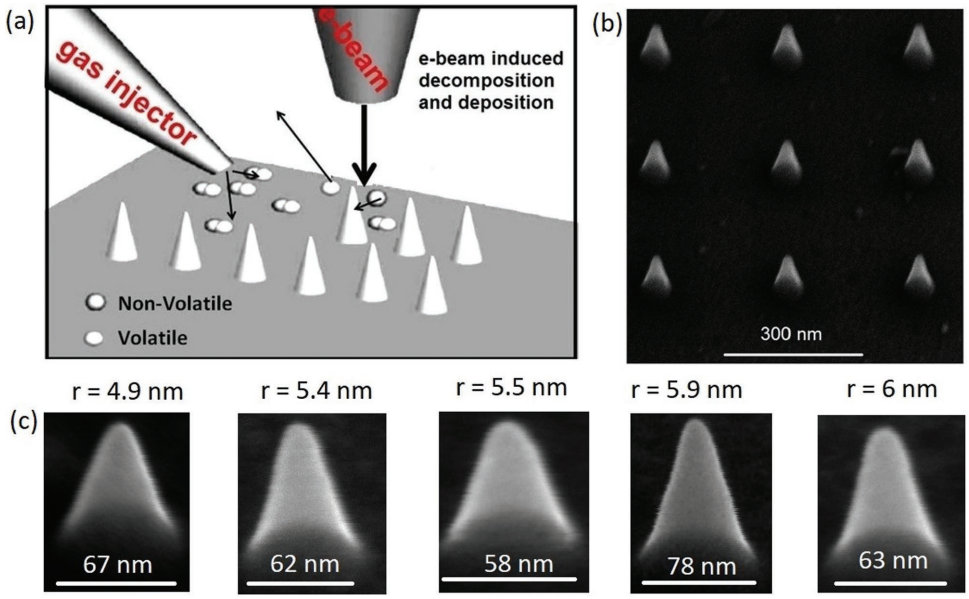

Figure 4. a) Schematic of the EBID of Pt nanocones. The volatile part of the decomposed precursor is ejected and the nonvolatile part (mainly Pt) deposit on the substrate forming nanocones. b) SEM image of nanocone arrays. c) SEM viewgraph of representative nanocone structures. The values of the radius of curvature and of the base are also indicated.

estimated local pressure on the sample) (10^{-6} Torr) with an estimated deposition rate of 10^{18}–10^{19} molecules cm^2 s^{-1}. The nanocone base diameter is adjusted by changing the scanning pattern and the height by varying number of scan cycles during electron beam rastering.

The interaction of the e-beam with the precursor leads to the dissociation and deposition of the gas molecules due to energy transfer and also to the reduction of Pt due to charge transfer. The volatile part (organic part) of the decomposed precursor is ejected from the chamber through the vacuum system and the nonvolatile part (mainly Pt and carbon) deposits on the substrate (see schematic **Figure** 4a). Since the e-beam can be focused to a sub-nanometer scale, the deposited structure size can be manipulated to achieve the desired size. The technique needs accurate focusing of the e-beam to obtain a good spatial resolution. The shorter exposure time required to define the structures (less than 5 s per cone) permits the fabrication of large arrays of nanocones in less than an hour. This makes the approach comparable with other techniques that allow parallel fabrication of single nanostructures. Hence, quality and quantity can also be well maintained. The fabricated nanocones are perfectly right-circular cones, with smooth side walls (see Figure 4b,c). Furthermore, this technique allows the fabrication of nanocones with a tip radius of curvature below 6 nm (mean value equal to 5.8 ± 0.1 nm) with a good reproducibility, if the e-beam is well focused (see Figure 4c; and also Figures S1 and S2 of the Supporting Information). Otherwise a defocused e-beam induced deposition results in a platinum tip radius of curvature of more than 10 nm (as shown in Figures S1 and S2 of the Supporting Information). The conducting nature of the deposited materials allows for in situ optical characterization of the nanocones during or after deposition.

In order to obtain nanocones with the required plasmonic properties, the structures were then covered with 25–30 nm of gold through sputtering deposition (as shown schematically in **Figure 5**a) and the sample was annealed in nitrogen flow at 180 °C for 20 min. The annealing procedure was performed in order to improve the nanocone quality by enlarging the grain sizes and increase the surface smoothness.[50] Parameters were optimized in order to have the best compromise between a smooth surface and a sharp nanocone tip. Figure 5b depicts the SEM image of gold nanocones after these steps. The typical radius of curvature of 30 nm gold layer thick nanocone was below 10 nm (mean value equal to 9.4 ± 1.0 nm). For example, Figure 5c shows a plasmonic nanocone with a tip radius of curvature around 6 nm. The radius of curvature and the overall shape of the cones depend on the thickness of the deposited gold layer. The radius of curvature increase with increasing the thickness of gold layer (see Figures S3–S5 of the Supporting Information). The typical radius of curvature was 16 ± 0.7 nm for 40 nm gold layer and 18 ± 1.7 nm for 50 nm thick gold layer.

If desired, it is possible to remove the gold layer deposited on the substrate using FIB milling (not shown).

Spectroscopy of Individual Nanostructures: Dark-field illumination and collection can effectively separate the weak scattering signal of a nanocone from the excitation source making this approach suitable for spectroscopy of single plasmonic nanostructures.[51] The optical characterization (Rayleigh scattering) has been performed using a homemade dark-field spectroscopy setup, where the nanostructures are excited using a high numerical aperture (NA) microscope objective at large incident angles, and the scattered light is collected by a lower NA

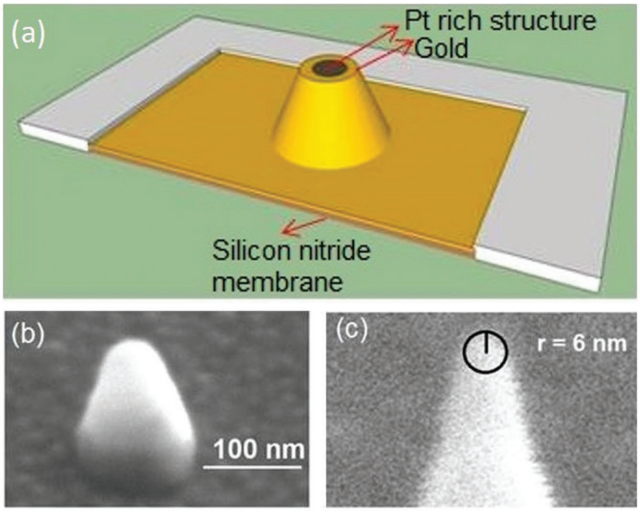

Figure 5. a) Schematics of a truncated nanocone (not in scale). b) SEM image of plasmonic gold nanocone. c) The tip radius of curvature can be made as small as 6 nm.

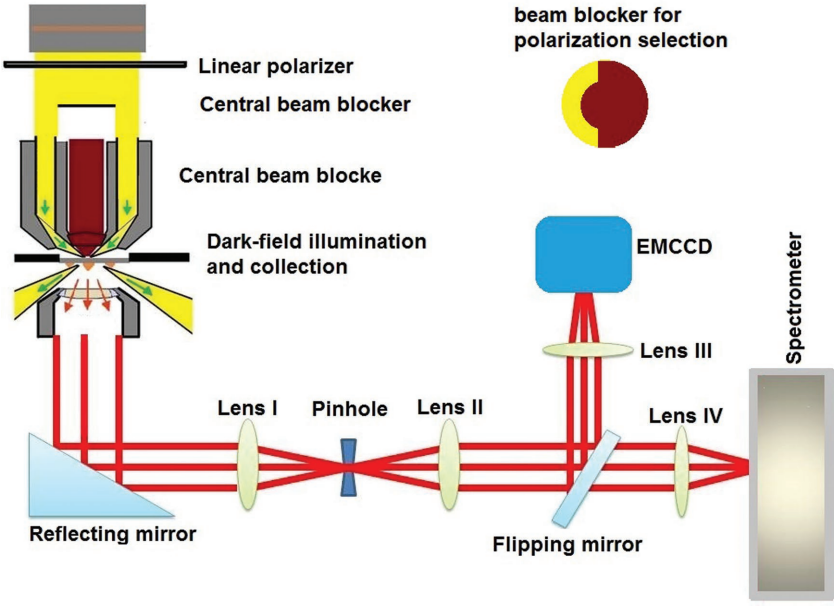

Figure 6. Schematic of the experimental setup for dark-field microscopy of plasmonic nanocones. Inset: schematics of the beam blocker used to create a longitudinal polarization in the focal spot of the microscope objective.

microscope objective at smaller angles to avoid the excitation source. The experimental setup is schematically shown in **Figure 6**.

A collimated broadband white light source (Ocean Optics Halogen light source, HL-2000-FHSA) has been linearly polarized and its orientation adjusted via a half-wave plate. A hollow-cone of polarized light (cone angle 53.1°–64.2°) is then focused on the sample using a central beam blocker and a high-NA microscope objective (Olympus LMPlanFl 100 X, 0.8/0.9 NA) for dark-field illumination. The polarization of the focused field is manipulated by blocking part of the hollow-cone of light. For instance, while a linearly polarized annular beam yields s-polarization in the focus (electric field parallel to the substrate and perpendicular to the long axis of the cone), by blocking some parts of the annular aperture (e.g., when half of it is blocked as shown in Figure 6) s- and p-polarization (electric field perpendicular to the substrate and parallel to the long axis of the cone) can be achieved. This work is interested in the long-axis mode (excited by p-polarized light) as it can strongly enhance single emitters.[26]

The light scattered by the nanocone was collected (collection angle was between 30° and 53.1°) by a lower NA microscope objective (Olympus MPlanFLN X 50/60, 0.8–0.5 NA). The NA has been chosen to avoid the incident light that comes at a maximum angle of 64.2° (see Figure 6). Then the collected signal was sent to an EMCCD camera (Princeton Instruments, ProEM-HS: 512 BX3, back-illuminated EMCCD, more than 90% quantum efficiency in the NIR region) for dark-field imaging. Imaging was performed using a flippable reflecting mirror that is placed in front of the spectrometer as shown in Figure 6. The mirror can be switched to get access to the spectrometer to measure the LSPRs. The spectrometer (Horiba, T64000) is equipped with a Synapse CCD (JOBIN YVON, front illuminated open electrode 1024 × 256 CCD). The quantum efficiency of the CCD in the NIR region is around 40–50%. During a single nanocone measurement the collected light is focused into a pinhole to be sure that the signal comes from only one cone.

Although the background intensity is minimal in the dark-field configuration, the measured signal (I_n) must be corrected for the weak scattering by the substrate (I_b). It must also be adjusted for the uneven white light illumination across the broad wavelength range (I_{wl}). It is also important to consider the dark counts of the detector (I_{dc}) (i.e., the spectrum when the lamp is turned off). The scattered signal (I) from the nanocone is thus obtained by $I = (I_n - I_b)/(I_{wl} - I_{dc})$ and it resembles a Lorentzian peak with a resonance wavelength dependent on the nanocone base and height.

Simulations and Theory: The possible dimensions (base and height or aspect ratio) of gold nanocones that yield the plasmon resonance in the NIR were previously studied.[26] In the NIR region, where the dissipation in gold becomes smaller, the enhancement of the spontaneous emission rate of quantum emitters can reach more than three orders of magnitude, while the antenna efficiency can be as large as 80%.[26] Here, this work performed body-of-revolution finite-difference time-domain calculations in order to assess how the thickness of the gold layer and the platinum–carbon based core affect the spontaneous emission rate and the antenna efficiency near resonance, as well as the spectral position of the LSPR.

The inset of **Figure 7**a shows an electric dipole source oriented along the symmetry axis of the nanocone is placed at a distance of 10 nm from the tip with a radius of curvature of 10 nm. That effectively excites the longitudinal plasmon mode of the nanocone. This is similar to the p-polarization excitation scheme in the homemade setup. The nanocone is in air and the platinum-based nanocone has a fixed base and height of 110 nm. The thickness of a gold layer (yellow) on the platinum–carbon based nanocone (black) is changed from 30 to –55 nm. The base of the nanocone is on a substrate that has the same index of refraction as the one used in the experiments. The radiative decay rate enhancement is calculated as the ratio of the power radiated by the dipole in the

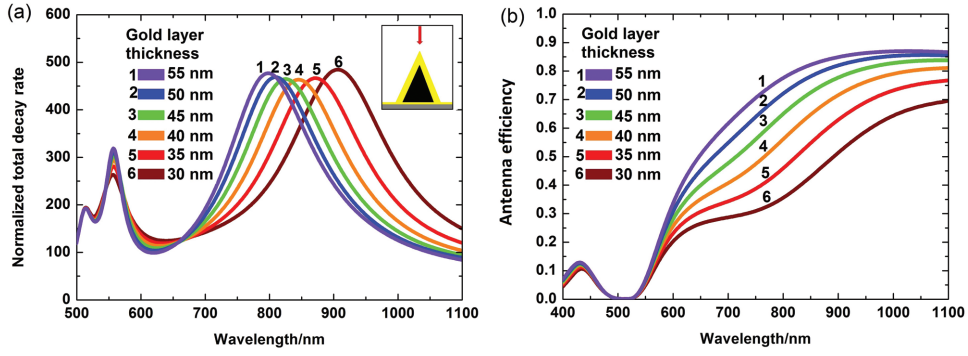

Figure 7. a) Total decay rate enhancement as a function of wavelength for a quantum emitter coupled to plasmonic gold nanocones as shown in the inset, where the dipole emitter is indicated by a red arrow. b) Antenna efficiency as a function of wavelength.

presence of the nanocone to the power radiated by the dipole in free space. The antenna efficiency is calculated as the ratio of the power radiated to the far-field to the total power emitted by the dipole with unity quantum efficiency in the presence of the nanocone.[26]

Figure 7a shows that nanocone with this dimension exhibits a LSPR in the NIR region enabling indeed more than two orders of magnitude enhancement in the total decay rate. However, the platinum–carbon core reduces the antenna efficiency due to its large absorption in the NIR, but this effect can be largely mitigated by increasing the thickness of the gold layer, as shown in Figure 7b. Since the platinum–carbon composite material has a large refractive index, screening the core with thicker gold layer results in a blueshift of the LSPR. The decrease in the aspect ratio of the nanocone as the result of an increase in gold layer thickness also contributes to the blueshift of the LSPR.

Supporting Information

Supporting Information is available from the Wiley Online Library or from the author.

Acknowledgements

The authors gratefully acknowledge financial support by the University of Siegen, Germany, and the Italian Institute of Technology (IIT), Italy, and the COST Action MP1403 "Nanoscale Quantum Optics" for stimulating discussions. The research leading to these results has also received funding from the European Research Council under the European Union's Seventh Framework Programme (FP/2007-2013)/ERC Grant Agreement n. [616213], CoG: Neuro-Plasmonics.

Conflict of Interest

The authors declare no conflict of interest.

Keywords

dark-field spectroscopy, electron beam-induced deposition, localized surface plasmons, nanofabrication, plasmonic gold nanocones

Received: June 21, 2017
Revised: July 27, 2017
Published online:

[1] A. Imamoglu, D. Awschalom, G. Burkard, D. P. DiVincenzo, D. Loss, M. Sherwin, A. Small, *Phys. Rev. Lett.* **1999**, *83*, 4204.
[2] S. Uppuluri, E. Kinzel, Y. Li, X. Xu, *Opt. Express* **2010**, *18*, 7369.
[3] B. Knoll, F. Keilmann, *Nature* **1999**, *399*, 134.
[4] D. Yelin, D. Oron, S. Thiberge, E. Moses, Y. Silberberg, *Opt. Express* **2003**, *11*, 1385.
[5] P. Zijlstra, P. M. R. Paulo, M. Orrit, *Nat. Nanotechnol.* **2012**, *7*, 379.
[6] M. Fleischer, A. Weber-Bargioni, M. V. P. Altoe, A. M. Schwartzberg, P. J. Schuck, S. Cabrini, D. P. Kern, *ACS Nano* **2011**, *5*, 2570.
[7] Y. Gong, J. Vučković, *Appl. Phys. Lett.* **2007**, *90*, 033113.
[8] K. J. Vahala, *Nature* **2003**, *424*, 839.
[9] J. P. Reithmaier, G. Sek, A. Löffler, C. Hofmann, S. Kuhn, S. Reitzenstein, L. V. Keldysh, V. D. Kulakovskii, T. L. Reinecke, A. Forchel, *Nature* **2004**, *432*, 197.
[10] A. Flatae, T. Grossmann, T. Beck, S. Wiegele, H. Kalt, *APL Mater.* **2014**, *2*, 012107.
[11] M. Nomura, N. Kumagai, S. Iwamoto, Y. Ota, Y. Arakawa, *Nat. Phys.* **2010**, *6*, 279.
[12] R. Chikkaraddy, B. de Nijs, F. Benz, S. J. Barrow, O. A. Scherman, E. Rosta, A. Demetriadou, P. Fox, O. Hess, J. J. Baumberg, *Nature* **2016**, *535*, 127.
[13] M. Agio, A. Alù, *Optical Antennas*, Cambridge University Press, New York **2013**.
[14] M. I. Stockman, *Phys. Today* **2011**, *64*, 39.
[15] W. A. Murray, W. L. Barnes, *Adv. Mater.* **2007**, *19*, 3771.
[16] Y. J. Lu, J. Kim, H. Y. Chen, C. Wu, N. Dabidian, C. E. Sanders, C. Y. Wang, M. Y. Lu, B. H. Li, X. Qiu, W. H. Chang, L. J. Chen, G. Shvets, C. K. Shih, S. Gwo, *Science* **2012**, *337*, 450.
[17] T. B. Hoang, G. M. Akselrod, C. Argyropoulos, J. Huang, D. R. Smith, M. H. Mikkelsen, *Nat. Commun.* **2015**, *6*, 7788.
[18] S. Kühn, U. Håkanson, L. Rogobete, V. Sandoghdar, *Phys. Rev. Lett.* **2006**, *97*, 017402.
[19] F. Tam, G. P. Goodrich, B. R. Johnson, N. J. Halas, *Nano Lett.* **2007**, *7*, 496.
[20] C. Belacel, B. Habert, F. Bigourdan, F. Marquier, J. P. Hugonin, S. Michaelis de Vasconcellos, X. Lafosse, L. Coolen, C. Schwob, C. Javaux, B. Dubertret, J. J. Greffet, P. Senellart, A. Maitre, *Nano Lett.* **2013**, *13*, 1516.
[21] M. Thomas, J. J. Greffet, R. Carminati, J. R. Arias-Gonzalez, *Appl. Phys. Lett.* **2004**, *85*, 3863.
[22] A. V. Shchegrov, K. Joulain, R. Carminati, J. J. Greffet, *Phys. Rev. Lett.* **2000**, *85*, 1548.
[23] K. Matsuzaki, S. Vassant, H. W. Liu, A. Dutschke, B. Hoffmann, X. Chen, S. Christiansen, M. R. Buck, J. A. Hollingsworth, S. Götzinger, V. Sandoghdar, *Sci. Rep.* **2017**, *7*, 42307.
[24] A. Kinkhabwala, Z. Yu, S. Fan, Y. Avlasevich, K. Müllen, W. E. Moerner, *Nat. Photonics* **2009**, *3*, 654.
[25] A. G. Curto, G. Volpe, T. H. Taminiau, M. P. Kreuzer, R. Quidant, N. F. van Hulst, *Science* **2010**, *329*, 930.
[26] A. Mohammadi, F. Kaminski, V. Sandoghdar, M. Agio, *J. Phys. Chem. C* **2010**, *114*, 7372.
[27] M. Fleischer, D. Zhang, K. Braun, S. Jäger, R. Ehlich, M. Häffner, C. Stanciu, J. K. Hörber, A. J. Meixner, D. P. Kern, *Nanotechnology* **2010**, *21*, 065301.
[28] C. M. Hsu, S. T. Connor, M. X. Tang, Y. Cui, *Appl. Phys. Lett.* **2008**, *93*, 133109.
[29] B. Hoffmann, S. Vassant, X. W. Chen, S. Götzinger, V. Sandoghdar, S. Christiansen, *Nanotechnology* **2015**, *26*, 404001.
[30] W. Wu, M. Hu, F. S. Ou, Z. Li, R. S. Williams, *Nanotechnology* **2010**, *21*, 255502.
[31] J. M. Kontio, J. Simonen, J. Tommila, M. Pessa, *Microelectron. Eng.* **2010**, *87*, 1711.
[32] T. Kim, J. Kim, S. J. Son, S. Seo, *Nanotechnology* **2008**, *19*, 295302.
[33] F. De Angelis, C. Liberale, M. L. Coluccio, G. Cojoc, E. Di Fabrizio, *Nanoscale* **2011**, *3*, 2689.
[34] M. Böhmer, J. Enderlein, *J. Opt. Soc. Am. B* **2003**, *20*, 554.
[35] G. V. Hartland, *Chem. Rev.* **2011**, *111*, 3858.
[36] M. Liu, M. Pelton, P. Guyot-Sionnest, *Phys. Rev. B* **2009**, *79*, 035418.
[37] K. Munechika, J. M. Smith, Y. Chen, D. S. Ginger, *J. Phys. Chem. C* **2007**, *111*, 18906.
[38] W. Demtroder, *Laser Physics: Basic Concepts and Instrumentation*, Springer-Verlag, Berlin **1982**.
[39] P. B. Johnson, R. W. Christy, *Phys. Rev. B* **1972**, *6*, 4370.
[40] E. D. Palik, *Handbook of Optical Constants of Solids*, Academic Press, New York **1985**.
[41] M. Z. Quinten, *Phys. B: Condens. Matter* **1996**, *101*, 211.
[42] M. M. Alvarez, J. T. Khoury, T. G. Schaaff, M. N. Shafigullin, I. Vezmar, R. L. Whetten, *J. Phys. Chem. B* **1997**, *101*, 3706.
[43] C. Sönnichsen, T. Franzl, T. Wilk, G. von Plessen, J. Feldmann, O. Wilson, P. Mulvaney, *Phys. Rev. Lett.* **2002**, *88*, 077402.

[44] L. Wimmer, G. Herink, D. R. Solli, S. V. Yalunin, K. E. Echternkamp, C. Ropers, *Nat. Phys.* **2014**, *10*, 432.
[45] M. Krüger, M. Schenk, P. Hommelhoff, *Nature* **2011**, *475*, 78.
[46] C. Ropers, D. R. Solli, C. P. Schulz, C. Lienau, T. Elsaesser, *Phys. Rev. Lett.* **2007**, *98*, 043907.
[47] V. Kravtsov, R. Ulbricht, J. M. Atkin, M. B. Raschke, *Nat. Nanotechnol.* **2016**, *11*, 459.
[48] X. Chen, A. Mohammadi, A. H. B. Ghasemi, M. Agio, *Mol. Phys.* **2013**, *111*, 3003.
[49] R. Narayanan, M. A. El-Sayed, *Nano Lett.* **2004**, *4*, 1343.
[50] K. Chen, V. P. Drachev, J. D. Borneman, A. V. Kildishev, V. M. Shalaev, *Nano Lett.* **2010**, *10*, 916.
[51] M. Hu, C. Novo, A. Funston, H. Wang, H. Staleva, S. Zou, P. Mulvaney, Y. Xia, G. V. Hartland, *J. Mater. Chem.* **2008**, *18*, 1949.